Electrostatic Self-Assembly of Oppositely Charged Copolymers and Surfactants: A Light, Neutron, and X-ray Scattering Study

Jean-François Berret,* Brigitte Vigolo, Ronny Eng, and Pascal Hervé

Complex Fluids Laboratory, CNRS-Cranbury Research Center Rhodia Inc., 259 Prospect Plains Road, Cranbury, New Jersey 08512

Isabelle Grillo

Institute Laue-Langevin, BP 156, F-38042 Grenoble Cedex 9, France

Lin Yang

Brookhaven National Laboratory, Upton, New York 11973

Received January 16, 2004; Revised Manuscript Received April 16, 2004

ABSTRACT: We report on the formation of colloidal complexes resulting from the electrostatic self-assembly of polyelectrolyte−neutral diblock copolymers and oppositely charged surfactant. The copolymers investigated are asymmetric and characterized by a large neutral block. Using light, neutron, and X-ray scattering experiments, we have shown that the colloidal complexes exhibit a core−shell microstructure. The core is described as a dense microphase of micelles connected by the polyelectrolyte blocks, whereas the shell is a diffuse brush made from the neutral chains. For all copolymer/surfactant systems, we show the existence of a critical charge ratio Z_C (∼1) above which the formation of hierarchical structures takes place. Copolymers of different molecular weight and polyelectrolyte blocks have been studied in order to assess the analogy with another type of core−shell aggregates, the polymeric micelles made from amphiphilic copolymers. The present results indicate that the radius of the core depends essentially on the degree of polymerization of the polyelectrolyte block and not on that of the neutral chain. On the other hand, the size of the overall colloid increases with increasing molecular weights of the copolymers. Taking advantage of the resolution of X-ray scattering, we have also shown that the micelles in the core of the aggregates are structurally disordered.

I. Introduction

During the past decade, there has been a widespread interest for the design and synthesis of a new polymer-based colloidal particles of high stability in aqueous solutions.[1] Among these particles, colloidal complexes have emerged as a new type of microstructure with potential applications in detergency, catalysis, and drug delivery. Colloidal complexes result from a self-assembly mechanism between polyelectrolyte−neutral block copolymers and oppositely charged species. The block copolymer, also called double hydrophilic copolymer,[2] is the key feature of the electrostatic self-assembly. The overall size and stability of the colloid depend on the nature of electrostatic charges, on the molecular weight, and on the flexibility of the chains. The first macromolecules or macroions having been complexed with double hydrophilic copolymers were synthetic and biological macromolecules,[3,4] proteins,[5,6] and surfactant micelles.[7−9] Since these first studies, the formation of stable complexes has been demonstrated using multivalent counterions[10,11] and mineral nanoparticles.[12] Recently, Jeong et al. have shown that colloidal complexes made from antisense nucleotide diblocks and cationic fusogenic peptide can be used as a novel intracellular delivery system.[13] In this later example, the diblock is a short DNA segment covalently bound to a poly(ethylene oxide) chain.

From the earlier works,[2,3,5,9,14,15] it was recognized that the colloids exhibit a core−shell structure. The core is described as a complex coacervation microphase, and it is made from the oppositely charged macromolecules or macroions. The corona is made from the neutral chains and ensures the stability of the whole particle. From its microstructure, these colloids resemble the well-known amphiphilic block copolymer micelles.[1] Their originality relies however on the possibility to associate components of different nature, such as organic and inorganic or synthetic and biological.

In the present paper, we deal with the structure and the stability of colloidal complexes made from oppositely charged block copolymers and surfactants. In a previous study, we reported on the structure of the colloidal particles using poly(sodium acrylate)-*b*-poly(acrylamide) as anionic−neutral copolymer and dodecyltrimethylammonium (DTAB) as cationic surfactant.[15,16] We have found that the core is constituted from densely packed micelles connected by the polyelectrolyte blocks. We also suggested that the structure of the core is reminiscent of that of the precipitate obtained by mixing homopolyelectrolyte and surfactant. (For recent theoretical modeling of the phase behaviors of oppositely charged polymer/surfactant mixtures, see refs 17−19.) In a second study, we presented Monte Carlo simulations that allowed us to estimate the number of surfactant micelles per aggregate (∼100).[20] A schematical representation of the colloidal complexes made from diblocks and surfactants is displayed in Figure 1. In the present paper, we show that complexes form in various conditions, i.e., using weak or strong polyelectrolytes as well as using positively or negatively charged blocks. We investigate different molecular weights for the charged

* Corresponding author. E-mail: jeanfrancois.berret@us.rhodia.com.

10.1021/ma0498722 CCC: $27.50
Published on Web 05/29/2004

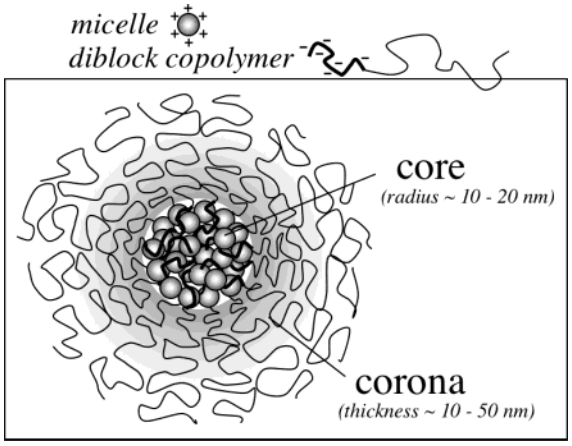

Figure 1. Representation of a colloidal complex formed through the association of oppositely charged block copolymers and surfactants. The core is described as a complex coacervation microphase of micelles connected by the polyelectrolyte blocks. The corona is made of the neutral segments. Depending on the copolymer molecular weight, the radius of the core ranges from 10 to 20 nm and the corona thickness between 10 and 50 nm.

and neutral segments by means of scattering techniques and derive qualitative laws of variation for the overall core and corona dimensions. The present data are compared to the scaling found for amphiphilic block copolymers.

II. Experimental Section

II.1. Material, Polymer Characterization, and Sample Preparation. In the present survey, we report on different block copolymers/surfactant systems. The polyelectrolyte blocks of the diblock structures are either poly(sodium acrylate), poly(styrene sodium sulfonate), or poly(trimethylammonium ethyl acrylate methyl sulfate). This later polymer is sometimes referred to as poly{[2-(acryloyloxy)ethyl]trimethylammonium methyl sulfate} in the literature.[21] For all copolymers studied, the neutral block is a poly(acrylamide) chain. The four polymers aforementioned are abbreviated in the following as PANa, PSS, PTEA, and PAM, respectively, yielding for the copolymer structures PANa-*b*-PAM, PSS-*b*-PAM, and PTEA-*b*-PAM. The synthesis of these copolymers is based on the Madix technology, which uses the xanthate as chain-transfer agent in the controlled radical polymerization.[22,23]

PANa is a weak polyelectrolyte whose ionization depends on the pH. All the experiments were conducted at neutral pH where it is expected that most of the monomers are charged. Two molecular weights were studied, 1000 and 5000 g mol^{-1}. To investigate the role of the neutral block on the formation of complexes, block copolymers with different PAM molecular weights were targeted: 5000, 10 000, 30 000, and 60 000 g mol^{-1}. As a whole, we had four different copolymers at our disposal: PANa (1000 g mol^{-1})-*b*-PAM (5000 g mol^{-1}), PANa (1000 g mol^{-1})-*b*-PAM (10 000 g mol^{-1}), PANa (5000 g mol^{-1})-*b*-PAM (30 000 g mol^{-1}), and PANa (5000 g mol^{-1})-*b*-PAM (60 000 g mol^{-1}). In the following, the copolymers will be named by their degree of polymerization, PANa (1000 g mol^{-1})-*b*-PAM (5000 g mol^{-1}) becoming then PANa(14)-*b*-PAM(70). PSS and PTEA are strong polyelectrolytes, and in aqueous solutions the ionization of the chains is assumed to be complete. With molecular weights 7000 and 11 000 g mol^{-1}, respectively, these charged chains were linked by MADIX to a 30 000 g mol^{-1} PAM, yielding for final structures PSS(33)-*b*-PAM(420) and PTEA(41)-*b*-PAM(420). Table 1 recapitulates the chemical formula and molecular weights of the copolymers investigated in this study.

Static and dynamic light scattering experiments were performed on the copolymers solutions (i.e., without surfactant) in order to determine the weight-average molecular weight M_W and the mean hydrodynamic radius R_H of the chains. The experimental conditions for these measurements are detailed in the next section. Data for M_W and R_H as well as the refractive index increment dn/dc are listed in Table 1. Except for PSS(33)-*b*-PAM(420), the molecular weights obtained are in good agreement with those targeted by the synthesis. The polydispersity index was estimated on two diblocks, PANa(69)-*b*-PAM(420) and PANa(69)-*b*-PAM(420) using size exclusion chromatography (SEC), and it was found around 1.6. Figure 2 shows the evolution of the hydrodynamic radius as a function of the molecular weight. The straight line in the double-logarithmic scale indicates a power law dependence of the form $R_H = 0.114M_W^{0.58}$, where R_H is expressed in Å and M_W in g mol^{-1}. The exponent 0.58 is in fair agreement with the predictions for polymers in good solvent conditions.[24]

The anionic copolymers PANa-*b*-PAM and PSS-*b*-PAM were investigated in solutions with positively charged surfactant dodecyltrimethylammonium bromide (DTAB), whereas the cationic copolymer PTEA(41)-*b*-PAM(420) was studied with the negatively charged sodium dodecyl sulfate (SDS). DTAB and SDS were purchased from Sigma and used without further purification. The critical micellar concentrations are 0.46 wt % (15 mmol L^{-1}) for DTAB and 0.23 wt % (8 mmol L^{-1}) for SDS. For comparison, we have also investigated polyelectrolyte homopolymers PANa(420) and PTEA(41), corresponding to molecular weights 30 000 and 11 000 g mol^{-1} respectively. The poly(acrylic acid) was obtained from Aldrich, and the charging of the chains was done by titration with sodium hydroxide. Poly(trimethylammonium ethyl acrylate methyl sulfate) homopolyelectrolyte, on the other hand, is an aliquot removed during the synthesis of the PTEA(41)-*b*-PAM(420) diblock, at the end of the synthesis of the first block.

Mixed solutions of surfactant and polymer were prepared by mixing a surfactant solution to a polymer solution, both prepared at the same concentration c (wt %). The relative amount of each component is monitored by the parameter defined in our previous papers as the stoichiometric ratio for chargeable groups, noted Z. As an example, for PANa(14)-*b*-PAM(70), Z = [S]/(14[P]), where [S] and [P] are the molar concentrations for the surfactant and for the polymer, respectively. $Z = 1$ describes an isoelectric solution, which is a solution characterized by the same number densities of positive and negative chargeable ions. The description of the mixed solutions in terms of c and Z is important since it allows to compare polymers with different structures and molecular weights. The parameter Z also appears to be a critical quantity in the formation of the colloidal complexes.

II.2. Experimental Techniques and Data Analysis. *Light Scattering.* Static and dynamic light scattering were performed on a Brookhaven spectrometer (BI-9000AT autocorrelator) for measurements of the Rayleigh ratio $R_\theta(q,\mathbf{c})$ and of the collective diffusion constant $D(\mathbf{c})$. The wave-vector q is defined as $q = (4\pi n/\lambda)\sin(\theta/2)$, where n is the refractive index of the solution, λ the wavelength of the incident beam (λ = 488 nm), and θ the scattering angle. Light scattering was used to determine the molecular weight of the different copolymers. In the dilute regime of concentrations (no interactions) and in a q range where their form factor is 1 ($q \leq 10^{-3}$ Å^{-1}), the concentration dependence of the Rayleigh ratio follows the expression

$$\frac{Kc}{R_\theta(c)} = \frac{1}{M_W} + 2A_2c \qquad (1)$$

In eq 1, $K = 4\pi^2n^2(\mathrm{d}n/\mathrm{d}c)^2/N_A\lambda^4$ is the scattering contrast coefficient, M_W is the weight-average molecular weight of the polymer, and A_2 is the second virial coefficient (N_A is the Avogadro number). The refractive index increment dn/dc was measured on a Chromatix KMX-16 differential refractometer at room temperature. Values of dn/dc are given in Table 1 for the different copolymers. They are in good agreement with the increments of the homopolymers themselves, PANa and PAM, for which one has dn/dc = 0.146 ± 0.10 cm^3 g^{-1} and dn/dc = 0.170 ± 0.10 cm^3 g^{-1}, respectively.[25] The formation of the

Table 1. Refractive Index Increment d*n*/d*c*, Weight-Average Molecular Weights M_W and Hydrodynamic Radius R_H of the Block Copolymers Studied in This Work[a]

polymers	M_W(PE), kg mol^{-1}	M_W(neutral), kg mol^{-1}	d*n*/d*c*, cm^3 g^{-1}	measured M_W, kg mol^{-1}	R_H, Å
PANa(14)-*b*-PAM(70)	1K	5K	n.d.	3.9 ± 0.2	18
PANa(14)-*b*-PAM(140)	1K	10K	n.d.	10.4 ± 1	24
PANa(69)-*b*-PAM(420)	5K	30K	0.157	43.5 ± 1	55
PANa(69)-*b*-PAM(840)	5K	60K	0.159	68.3 ± 2	79
PSS(33)-*b*-PAM(420)	7K	30K	0.158	86.6 ± 2	94
PTEA(41)-*b*-PAM(420)	11K	30K	0.153	44.4 ± 2	55

[a] The second and third columns show the molecular weights for each block (in kg mol^{-1}) targeted by the synthesis. The fifth column shows the weight-average molecular weight of the whole copolymer as determined from light scattering.

Table 2. Molecular Volume v_0 (in Å^3), Coherent Neutron Scattering Length Density ρ_N (in 10^{10} cm^{-2}), and Electronic Density ρ_X (in e Å^{-3}) of the Chemical Species Studied in This Work

species	chemical formula	v_0 (Å^3)	ρ_N (10^{10} cm^{-2})	ρ_X (e Å^{-3})
dodecyltrimethylammonium	$(C_{12}H_{25})-N^+(CH_3)_3$	447	−0.41	0.29
dodecyl sulfate	$(C_{12}H_{25})-OSO_3^-$	412	+0.30	0.35
acrylate	$CH_2CH-COO^-$	112	+1.81	0.33
acrylamide	$CH_2CH-CONH_2$	105	+1.56	0.36
styrene sulfonate	$CH_2CH-(C_6H_4)SO_3^-$	189	+2.48	0.50
trimethylammonium ethylacrylate	$CH_2CH-COO(C_2H_4)-N^+(CH_3)_3$	210	+0.68	0.41
water	H_2O	30	−0.56	0.33
deuterated water	D_2O	30	+6.38	0.33

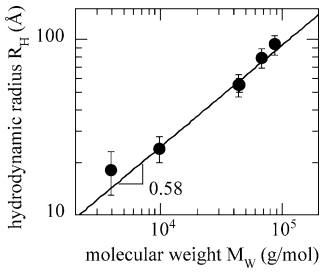

Figure 2. Molecular weight dependence of the hydrodynamic radius R_H for the six copolymers studied in this work. R_H is determined from dynamic light scattering on aqueous solutions at concentration 1 wt % and below. The list of the copolymers is given in Table 1. The straight line corresponds to the scaling $R_H = 0.114 M_W^{0.58}$.

colloidal complexes was followed for each copolymer/surfactant group by studying the Rayleigh ratio at $q = 2.3 \times 10^{-3}$ Å^{-1} ($\theta = 90°$) as a function of the *Z*. The collective diffusion coefficient $D(\mathbf{c})$ was measured in the range $c = 0.1-1$ wt %, and it was found to be concentration independent. From this value, the hydrodynamic radius of the colloids was calculated according to the Stokes−Einstein relation, $R_H = k_B T/6\pi\eta_0 D(\mathbf{c} \rightarrow 0)$, where k_B is the Boltzmann constant, *T* the temperature ($T = 298$ K), and η_0 the solvent viscosity ($\eta_0 = 0.89 \times 10^{-3}$ Pa s). The autocorrelation functions were analyzed by the cumulant technique, and the quadratic diffusion coefficient was considered for calculating R_H.

Small-Angle Neutron Scattering. Small-angle neutron scattering (SANS) was performed at the Laboratoire Léon Brillouin (LLB, Saclay, France) and at the Institute Laue-Langevin (ILL, Grenoble, France). The results between the different runs were found to be consistent with each others. Here, only data obtained on the beamlines D11 and D22 at ILL are shown. Copolymers/surfactant solutions were prepared at a concentration $\mathbf{c} = 1\%$ following the procedures described in the previous section. We have used D_2O as a solvent for contrast reasons. The list of the molecular volumes v_0 and coherent scattering length densities ρ_N of the chemical species studied in this work are given in Table 2. From this table, it appears that all chemical species have a good contrast with respect to D_2O and thus are expected to contribute to the total scattering cross section. On D22, the data collected at 2 and 14 m cover a range in wave-vector: 1.5×10^{-3} and 0.25 Å^{-1}, with an incident wavelength of 12 Å. On D11, three settings were used (1.1, 4.5, and 20 m) with a neutron wavelength of 8 Å and a wave-vector resolution $\Delta q_N/q$ of 10%. Δq_N is calculated from the distribution of neutron wavelengths in the incident beam. The spectra are treated according to the ILL and LLB standard procedures, yielding neutron scattering cross sections expressed in cm^{-1}. We recall that the expression of the intensity scattered by a dispersion of spherical and homogeneous particles of volume *V* and contrast $\Delta\rho = \rho_N - \rho_S$.[26]

$$\frac{d\sigma}{d\Omega}(q,c) = n(c)V^2\Delta\rho^2 S(q,c)F(q) \qquad (2)$$

where $n(c)$ is the number density of particles at concentration *c* and ρ_S the scattering length density of the solvent. $F(q)$ and $S(q,c)$ are the form and structure of the particles.

Small-Angle X-ray Scattering. Small-angle X-rays scattering (SAXS) runs were performed at the Brookhaven National Laboratory (Brookhaven, Upton, NY) on the X21 beamline. We used a wavelength of 1.76 Å for the incoming beam and the sample−detector distance of 1 m. With the detector in the off-center position, the accessible *q* range was 0.01−0.4 Å^{-1}, with a resolution $\Delta q_{fwhm}/q$ of 1.25%. Δq_{fwhm} denotes here the full width at half-maximum of diffraction peaks characterizing ordered structures. The data were treated so as to remove the contribution of the 1.5 mm glass capillaries and that of the solvent. The *q* scale was calibrated against silver behenate powder. Finally, we have added in Table 2 the list of the electronic densities ρ_X of the surfactants and monomers studied. Contrary to neutron scattering, the contrasts in X-ray (of monomers or surfactant with respect to the solvent) can be either positive or negative.

III. Results

III.1. Homopolyelectrolyte/Surfactant Structures Resolved by X-ray Scattering. Solutions of homopolyelectrolytes and oppositely charged surfactants at the stoichiometric ratio $Z = 1$ usually exhibit a macroscopic phase separation. This is the case for the two systems put under scrutiny here: PANa(420) and PTEA(41) when they are mixed with DTAB and SDS, respectively. Shortly after mixing, the polymer/surfactant solution becomes turbid, and after centrifugation it displays two well-separated phases. In the concentration range explored here, the lower phase is a white precipitate whereas the upper phase is fluid and transparent. Figure 3 shows the X-ray scattering intensities of the precipitate obtained with PANa(420) and DTAB at concentration $c = 2$ wt % and $Z = 1$. The numerous Bragg reflections observed between 0.1 and 0.3 Å^{-1} attest of the existence of a long-range order. The

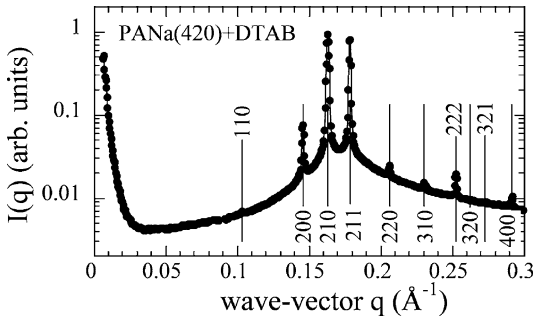

Figure 3. X-ray scattering intensity of the precipitate obtained by mixing poly(sodium acrylate) and dodecyltrimethylammonium bromide solutions at total concentration $c = 2$ wt % and at charge ratio $Z = 1$. The succession of Bragg peaks is consistent with a cubic structure of symmetry $Pm3n$. The lattice parameter of the elementary cell is 86.1 Å. The molecular weight of the polyelectrolyte is 30 000 g mol^{-1}, corresponding to 420 monomers.

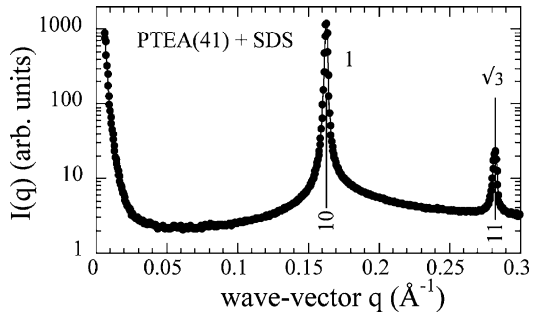

Figure 4. X-ray diffraction pattern of the precipitate obtained by mixing of poly(trimethylammonium ethyl acrylate methyl sulfate) and sodium dodecyl sulfate at total concentration $c =$ 15 wt % and at charge ratio $Z = 1$. The spacing ratio of the two Bragg peaks (1, $\sqrt{3}$) suggests an hexagonal structure.[32] The average distance between the cylindrical aggregates is 66.8 Å. The molecular weight of the polyelectrolyte is 11 000 g mol^{-1}, corresponding to 41 monomers.

sequence of Bragg peaks in Figure 3 is interpreted as arising from a cubic structure associated with the space group of symmetry $Pm3n$.[27−31] Classical for surfactant/polymer mesophases, the $Pm3n$ structure bears some similarities with the face-centered-cubic structure (fcc, space group $Fm3m$). Its specificities are that each face of the cube representing a lattice cell possesses two surfactant micelles (instead of one for the fcc) and that the volume fraction of spheres is lower than that of the fcc structure, 0.524 instead of 0.74. For PANa(420)/DTAB precipitates, we are able to identify up to the tenth order of the diffraction pattern. From the position of the first-order peak at $q_{110} = 0.1033$ Å^{-1}, we find a lattice parameter of 86.1 Å. The cubic symmetry finally suggests that in the precipitates the surfactants are organized into spherical micelles, these micelles occupying the nodes of the cubic lattice.

Figure 4 shows the diffraction patterns of the precipitate obtained from a PTEA(41)/SDS solution prepared at total concentration $c = 15$ wt % and $Z = 1$. For this second system, the presence of Bragg peaks with spacing ratio 1, $\sqrt{3}$ suggests an hexagonal order. The SDS molecules are assumed to associate into elongated cylindrical micelles, i.e., in a structure that maintains the translational and orientational long-range orders. From the position of the first-order peak at $q_{10} = 0.1629$ Å^{-1}, we derive the average distance between cylinders of 66.8 Å ($4\pi/q\sqrt{3}$). Microscopic observations between crossed polarizers show that the PTEA(41)/SDS precipitates are strongly birefringent. X-ray data similar to those of Figure 4 have been reported recently on the ternary system PCMA/SDS/water,[32] where PCMA stands for poly(trimethylammonium ethyl acrylate chloride), a system that differs from ours only by the counterion. Note finally that, in the two cases of homopolymer/surfactant precipitates mentioned, it is assumed that the polyelectrolyte chains are wrapped on the surfactant aggregates, either spheres or cylinders, and connect them.[33,34] Since the same technique has been used for the characterization of the copolymer complexes, it was important to have the signatures of the precipitated phases as a comparison.

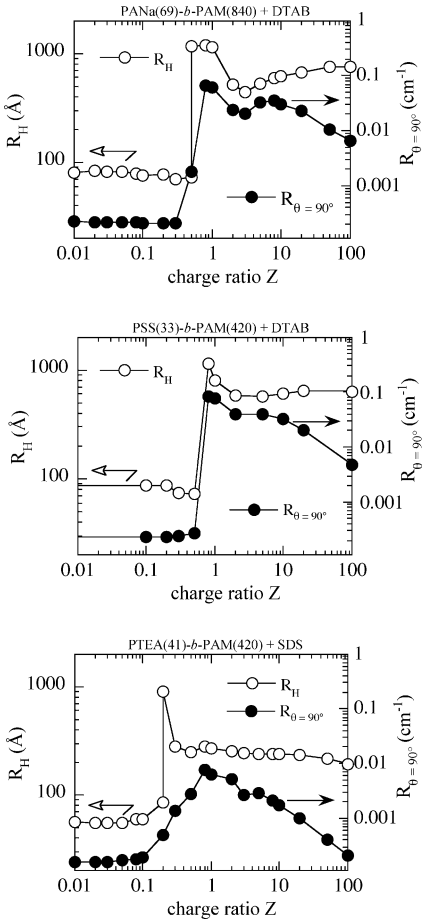

Figure 5. Evolution of the hydrodynamic radius R_H (left scale) and the Rayleigh ratio $R_\theta(q,\mathbf{c})$ (right scale) as a function of the charge ratio Z for (a) PANa(69)-*b*-PAM(840)/DTAB, (b) PSS(33)-*b*-PAM(420)/DTAB, and for (c) PTEA(41)-*b*-PAM(420)/SDS. Z is defined as the stoichiometric ratio for chargeable groups. The Rayleigh ratio is measured at $q = 2.3 \times 10^{-3}$ Å^{-1} ($\theta = 90°$). The total concentration in the solutions remains constant for values of Z ($c = 1$ wt %).

III.2. Evidence of a Critical Charge Ratio for the Complex Formation. Figure 5 displays the scattering properties of mixed solutions of block copolymers and oppositely charged surfactant at room temperature. These properties are the hydrodynamic radius R_H (left scale) and the Rayleigh ratio $R_\theta(q,\mathbf{c})$ at $q = 2.3 \times 10^{-3}$ Å^{-1} and $c = 1$ wt % (right scale). They are shown as a function of the charge ratio Z. We recall that $Z = 0$ stands for a solution with polymers only and $Z = \infty$ for a solution with surfactants only. Figure 5a−c shows data for PANa(69)-*b*-PAM(840), PSS(33)-*b*-PAM(420), and PTEA(41)-*b*-PAM(420), respectively, the two first copolymers being complexes with DTAB and the last one with SDS. The three plots exhibit the same overall

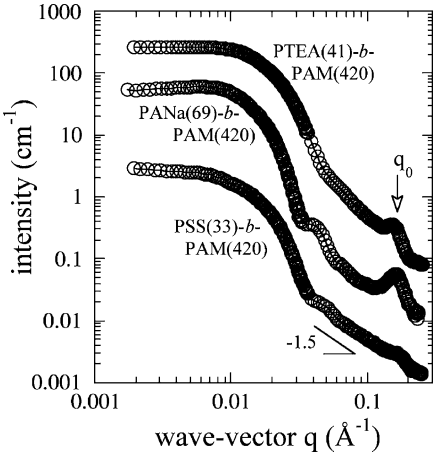

Figure 6. Neutron scattering intensities obtained from PANa(69)-*b*-PAM(420)/DTAB, PSS(33)-*b*-PAM(420)/DTAB, and PTEA(41)-*b*-PAM(420)/SDS aqueous solutions at $c = 1\%$ and $Z = 2$. For PSS(33)-*b*-PAM(420) and PTEA(41)-*b*-PAM(420), the intensities have been shifted for clarity (factor of $^1/_8$ and 8, respectively). An arrow indicates the position of the structure peak at $q_0 \sim 0.16$ Å^{-1}.

behavior. At low values of Z, typically below 0.1, the scattering intensity is independent of Z, and it remains at the level of the pure polymer. The hydrodynamic radii R_H are also close to those of single chains (Table 1). With increasing Z, there exists a critical charge ratio noted Z_C and comprised between 0.1 and 1, above which the Rayleigh ratio increases noticeably. $R_\theta(q,\mathbf{c})$ then levels off in the range $Z = 1-10$ and slowly decreases at higher Z values. Dynamical light scattering performed on solutions above Z_C reveals the presence of a purely diffusive relaxation mode associated with the Brownian diffusion of the particles.[15,16] Their hydrodynamic radii are calculated using the Stokes−Einstein relation, and for the three systems it is found that R_H remains nearly constant above Z_C. Their mean values are of the order of 500 Å for PANa(69)-*b*-PAM(840)/DTAB and PSS(33)-*b*-PAM(420)/DTAB and 250 Å for PTEA(41)-*b*-PAM-(420)/SDS. These values are ∼5 times larger the hydrodynamic radii of the single chains. As already noted in our previous work, close to Z_C, the autocorrelation function of the scattered light may detect two diffusive modes: a fast mode associated with the diffusion of single diblocks and one slow mode related to the diffusion of colloids of larger sizes. This is the case for the PTEA(41)-*b*-PAM(420)/SDS mixed solutions at $Z = 0.2$. In the range $Z = 1-10$, the analysis in terms of cumulant shows a relatively narrow polydispersity of sizes.[4,5] It is interesting to note that the polydispersity is narrower than that of the single diblocks. All these findings are in excellent agreement with those reported on PANa(69)-*b*-PAM(420)/DTAB.[15,16,20] Put all together, these results tend to prove the existence of unique behavior when block copolymers and oppositely charged surfactants are mixed in solutions, i.e., the formation of mixed colloidal complexes.

III.3. Microstructure of Colloidal Complexes by Small-Angle Scattering. Figure 6 compares the scattering cross sections of colloidal complexes obtained by SANS on the three systems PANa(69)-*b*-PAM(420)/DTAB, PSS(33)-*b*-PAM(420)/DTAB, and PTEA(41)-*b*-PAM(420)/SDS. The concentrations and charge ratios are the same for the three solutions, $c = 1$ wt % and $Z = 2$. Each data set is shifted with respect to each other by a multiplicative factor specified in the caption. The

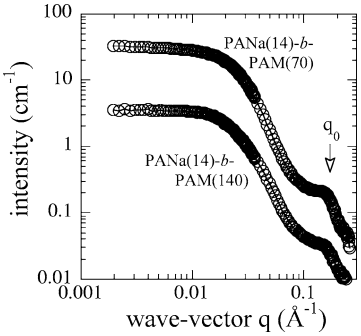

Figure 7. Comparison between PANa(14)-*b*-PAM(70)/DTAB and PANa(14)-*b*-PAM(140)/DTAB colloidal complexes, as measured by neutron scattering. The concentration is $c = 1$ wt % and $Z = 2$ for both systems. The intensity of the PANa(14)-*b*-PAM(70) solution is multiplied by 4.

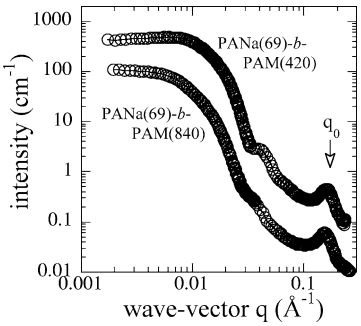

Figure 8. Same as Figure 7 for PANa(69)-*b*-PAM(420) and PANa(69)-*b*-PAM(840). The upper intensity is multiplied by 8.

solutions have been prepared in deuterated water, and we have checked that the change of solvent, from H_2O to D_2O, does not alter the complexation properties. In Figure 6, the scattering cross section is dominated by a strong forward scattering (i.e., at $q \to 0$) and by the appearance of a structure peak at high wave-vectors. This peak is located around $q_0 = 0.16$ Å^{-1} for the two systems with DTAB and around $q_0 = 0.15$ Å^{-1} for the system with SDS. Note that $2\pi/q_0 \sim 40$ Å corresponds to the distance between micelles in the core. The amplitude of this peak depends strongly on the type of polymers that is employed in the complex formation. For PSS(33)-*b*-PAM(420)/DTAB, it shows up as a weak bump that seems to be superimposed to a power law dependence of the form, $d\sigma/d\Omega \sim q^{-1.5}$. For PANa(69)-*b*-PAM(420)/DTAB, this peak is actually intense, and no power law can be detected in this q range. In our first reports, we had shown that the strong forward scattering and the structure peak at high wave-vectors are correlated and that they are the signatures of the form factor of the core−shell aggregates.[15,16,20] The power law mentioned previously is attributed to the corona made of the neutral blocks and surrounding the core.[35,36] This later aspect is discussed in the next section.

Figures 7 and 8 display the neutron scattering cross sections for the PANa-*b*-PAM/DTAB series of different molecular weights. In Figure 7, the SANS data obtained with copolymers PANa(14)-*b*-PAM(70) and PANa(14)-*b*-PAM(140) and DTAB are shown, whereas in Figure 8 the intensities displayed are those of PANa(69)-*b*-PAM(420) and PANa(69)-*b*-PAM(840), again complexed with DTAB. In each figure, the polyelectrolyte block is held constant, 1000 and 5000 g mol^{-1}, respectively, and the neutral block is allowed to change by a factor of 2.

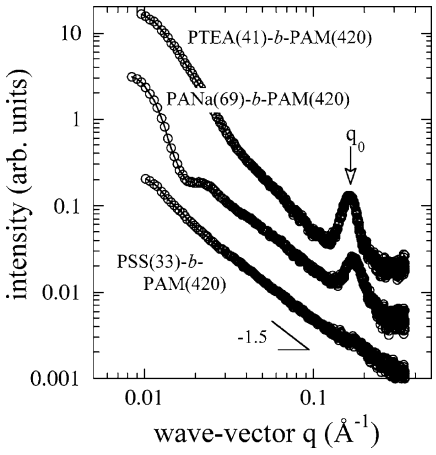

Figure 9. X-ray scattering intensities determined on the same solutions as those of Figure 6. For PANa(69)-*b*-PAM(420)/DTAB, PSS(33)-*b*-PAM(420)/DTAB, and PTEA(41)-*b*-PAM(420)/SDS, $c = 1$ wt % and $Z = 2$ and the solvent is D_2O. An arrow indicates the position of the structure peak at $q_0 \sim 0.16$ Å^{-1}.

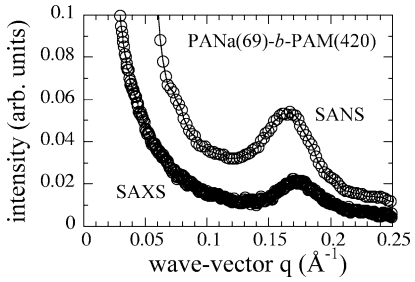

Figure 10. Comparison between the SANS and SAXS intensities obtained from PANa(69)-*b*-PAM(420)/DTAB complexes ($c = 1$ wt % and $Z = 2$ in D_2O). The structure peak at large wave-vectors appears equally broad in both techniques.

For the systems of Figure 7, the scattering is found to be independent or only weakly dependent on the molecular weight of the neutral block. Actually, if the data obtained for PANa(14)-*b*-PAM(70) would not have been shifted by a factor of 4, they would be superimposed to those of PANa(14)-*b*-PAM(140). The same holds for the copolymers of Figure 8. Comparing the systems with 1000 g mol^{-1} to a 5000 g mol^{-1} polyelectrolyte blocks reveals noticeable changes in the intensities and indicates the crucial role played by the charged block in the structure of the complexes.

The very same solutions investigated by neutron scattering and shown in Figure 6 were also studied with X-rays. Figure 9 display the X-ray intensity for PANa(69)-*b*-PAM(420)/DTAB, PSS(33)-*b*-PAM(420)/DTAB, and PTEA(41)-*b*-PAM(420)/SDS at $c = 1$ wt % and $Z = 2$, all solutions having been prepared in D_2O. For the three samples, the same typical features are apparent: a strong forward scattering, a structure peak around 0.16 Å^{-1}, and a power law dependence of the intensity at high q (exponents close to -1.5). It is interesting to note that as in neutron the structure peak in PSS(33)-*b*-PAM(420)/DTAB is again weak and hardly discernible, whereas for the two other systems it dominates the high q-region. For PANa(69)-*b*-PAM(420)/DTAB, the scattering exhibits a marked oscillation which minimum is located around 0.02 Å^{-1} (instead of 0.04 Å^{-1} in neutron).

Figures 10 and 11 display the previous intensities (those of PANa(69)-*b*-PAM(420)/DTAB and PTEA(41)-*b*-PAM(420)/SDS) in linear scale and in high q-region. This representation of the data emphasizes that the

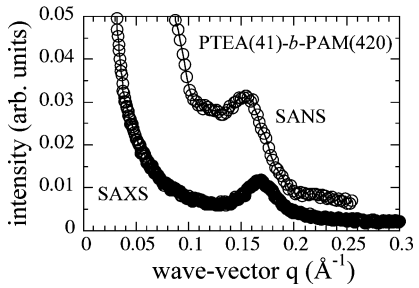

Figure 11. Same as in Figure 10 for the PTEA(41)-*b*-PAM(420)/SDS system.

intermicellar structure peak seen by X-rays is actually as broad as the one observed by neutrons (fwhm ~ 0.04 Å^{-1}). In both examples, it shows no internal substructures that could resemble those of Figures 3 and 4 or that could be indicative of micellar order in the core. One can also remark in Figures 10 and 11 that the X-ray peak is slightly shifted with respect to its position as determined by neutron scattering. This difference could originate in the different scattering contrasts exhibited by the aggregates with one or with the other technique.

IV. Analysis and Discussion

IV.1. Determination of the Core and Corona Sizes of the Complexes. It is probably useful to recall at this stage the experimental conditions under which the colloidal complexes are obtained. The concentrations that have been considered here are around 1 wt %, a choice dictated by the scattering experiments and by the requirements of good signal-to-noise ratios for the intensities. It is important to mention that for surfactant these concentrations are well above the critical association concentration (cac). For DTAB and PANa, the cac was estimated around 10^{-4} mol L^{-1}, corresponding to a weight concentration of 0.003 wt % (i.e., 30 ppm).[37] This value is 150 times lower than the cmc of the surfactant alone. Cac's of the order of 10^{-4} mol L^{-1} were also found for the PSS/DTAB and PTEA/SDS systems.[38] The complexation between the oppositely charged species is thus expected to take place in all the solutions studied here.[16]

The range around $c = 1$ wt % is interesting for a second reason. The particles that are formed at this concentration (either micelles or complexes) are not too numerous, and their mutual interactions have no or little effects on the scattering functions. In eq 2, this manifests itself by a structure factor equal to unity. The SANS and SAXS intensities displayed in this paper reflect therefore the form factors of the aggregates. The differences between intensities obtained by neutrons and by X-rays on the same solutions (as in Figures 6 and 9) result then from the different scattering contrasts of the elementary scatterers with respect to the solvent. As shown in Table 2, the difference $\rho - \rho_S$ can be either positive or negative, depending on the technique used. Starting from the structure depicted in Figure 1, it is possible to model the form factor of the aggregates. The first attempts to fit the scattering properties of complexes have used analytical expressions developed for polymeric micelles[11,12] or Monte Carlo methods to simulate the inner structure of the core.[20] In the case of the complexes there is another difficulty, which is that the exact microstructure of the core is not known. Because we are dealing with a multicomponent system (polymer, surfactant, counterion, and water),[34] it is not possible to know a priori the numbers of micelles and

Table 3. Characteristic Sizes of Colloidal Complexes Obtained from Oppositely Charged Block Copolymers and Surfactants[a]

polymer	surfactant	R_C (Å)	s	R_H (Å)
PANa(14)-*b*-PAM(70)	DTAB	65 ± 5	n.d.	130
PANa(14)-*b*-PAM(140)	DTAB	70 ± 5	n.d.	150
PANa(69)-*b*-PAM(420)	DTAB	128 ± 2	0.18	300
PANa(69)-*b*-PAM(840)	DTAB	146 ± 4	0.20	500
PSS(33)-*b*-PAM(420)	DTAB	108 ± 2	0.18	580
PTEA(41)-*b*-PAM(420)	SDS	84 ± 4	0.24	250

[a] R_C is the radius of the core, s is the polydispersity in core radius ($s = \sigma(R_C)/R_C$ where $\sigma(R_C)$ is the standard deviation), and R_H is the overall radius of the aggregates. The values for R_C and s were determined by neutron scattering (from solutions prepared with D_2O) and those for R_H by light scattering (from solutions prepared with H_2O). All the quantities in the table are for solutions at $c = 1$ wt % and $Z = 2$.

of polymers per aggregate. In the following, our analysis focuses on sizes rather than on aggregation numbers. This later aspect will be treated in a forthcoming paper.

The neutron scattering intensities at intermediate and low wave-vectors have been interpreted as arising from spherical and homogeneous particles. We assume a distribution of sizes characterized by the standard deviation $\sigma(R_C)$, where R_C is the mean radius of the distribution. This approach was shown to be appropriate for PANa(69)-*b*-PAM(420)/DTAB[15,16] as well as for PTEA(41)-*b*-PAM(420)/SDS[20] mixed solutions. It is also the case for the new mixed systems shown in Figures 6−8. Values of R_C and of the polydispersity $s = \sigma(R_C)/R_C$ are given in Table 3 for the six polymers studied ($c = 1$ wt % and $Z = 2$). For the solutions with the 1000 g mol^{-1} poly(sodium acrylate) block shown in Figure 7, the Porod representations could not be used to estimate the radius and polydispersity of the aggregates, as this was done with the other systems. Guinier adjustments were performed instead, and R_C was estimated from the radius of gyration. Summarizing Table 3, R_C is found to vary between 70 and 150 Å, with a typical polydispersity $s = 0.20$. When compared to the hydrodynamic radius, we observe that R_H is larger than R_C by a factor of 3−5. These findings agree with the core−shell microstructure. The contribution of the cores dominates the scattering measured by SAXS and by SANS, whereas the whole aggregate, including core and corona, appears in dynamic light scattering as a single particle of radius R_H.

In copolymer micelles, the contribution of the corona manifests itself at high wave-vectors as a power law of the form $d\sigma/d\Omega \sim q^{-1/\nu}$, where ν is the Flory exponent.[35,39] For Gaussian chains $\nu = 0.5$, which gives a q^{-2} decrease of the intensity, whereas for chains in good solvent $\nu = {}^3/_5$ and the intensity goes as $q^{-5/3}$. We found here similar dependences, especially for the PSS(33)-*b*-PAM(420)/DTAB system, which exhibits the largest corona among the six polymers studied. Scaling exponents of the order of −1.5 are in excellent agreement with the predictions for polymers in good solvent. Scaling laws at large q have been also reported in complexes made with multivalent counterions and nanoparticles.[11,12]

Finally, the present data allow to conclude about the structure of the core, an issue that could not be solved by neutron scattering because of the limited resolution. Is the core a disordered microphase of micelles, as the broad peak at q_0 seems to indicate it? Or is it an ordered phase which Bragg reflections are broadened by the reduced size of the crystallite? After all, the largest core

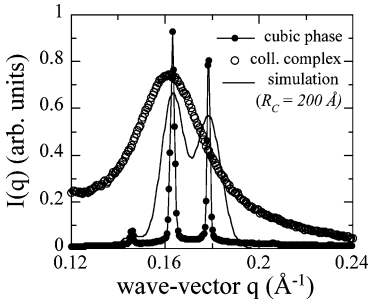

Figure 12. Comparison between X-ray intensities obtained for PANa(420)/DTAB precipitate and PANa(69)-*b*-PAM(420)/DTAB colloidal complexes with core radius $R_C = 200$ Å (not shown in Table 3). These large cores were obtained by mixing the initial polymer and surfactant solutions at high concentration.[16] The continuous line represents the Bragg reflections calculated for structurally ordered cores (space group $Pm3n$) of radius $R_C = 200$ Å.

size in Table 3 (that of PANa(69)-*b*-PAM(840)) corresponds to ∼8 micellar diameters. A well-ordered crystallite of size $2R_C$ would exhibit Braggs reflections characteristic of the crystal symmetry, but because of the reduced size of the scattering volume, each Bragg peak would be broadened up to a value $\Delta q_{fwhm} \sim 2.95/R_C$.[40] With $R_C \sim 100$ Å, one gets $\Delta q_{fwhm} = 0.03$ Å^{-1}. For the cubic phase with $Pm3n$ crystalline structure, the three main Bragg peaks are the (200), (210), and (211) reflections, with wave-vectors q comprised between 0.14 and 0.18 Å^{-1} (Figure 3). We can assume that in the case of an ordered core with the same symmetry these lines would also dominate the X-ray scattering intensity. These three reflections are separated however by ∼0.015 Å^{-1}, a distance that is lower than the $\Delta q_{fwhm} = 0.03$ Å^{-1} calculated previously. Thus, for cores of radius 100 Å, the three lines are expected to merge into a broader one, yielding a structure peak comparable to the one observed experimentally for the complexes. To clarify this issue, we need to find instances of complexes with large cores, at least larger than the ones listed in Table 3. In ref 16, we had shown that the sizes of the complexes depend noticeably on the mixing conditions of the initial polymer and surfactant solutions. We have established that mixing PANa(69)-*b*-PAM(420) and DTAB at concentrations as high as $c = 20$ wt % yields complexes with cores in the range $R_C = 200-250$ Å. The complexes are then diluted into the $c \sim 1$ wt % range for the scattering studies. Figure 12 displays the X-ray data of such complexes in the wave-vector range where the structure peak is apparent. Also shown are the (200), (210), and (211) Bragg peaks from Figure 3 and simulations assuming a broadening of these peaks by a quantity $\Delta q_{fwhm} \sim 2.95/R_C = 0.015$ Å^{-1}, now calculated using $R_C = 200$ Å. In this case, the broadened reflections do not merge and can still be separated. From this comparison we can conclude that the surfactant micelles located in the cores of the PANa-*b*-PAM/DTAB complexes are structurally disordered. The situation for the PTEA(41)-*b*-PAM(420)/SDS system is somewhat different since the cores do not display the hexagonal structure exhibited by the homopolyelectrolyte−surfactant precipitate[20] (Figure 4).

IV.2. Scaling Laws. Because polymeric micelles and colloidal complexes have the same core−shell microstructure, it is legitimate to ask whether the scaling properties found for copolymers in selective solvents could be relevant for the present systems. This analogy has been suggested recently for colloidal complexes

made with multivalent counterions[11,12] or with short homopolyelectrolyte chains.[41] For block copolymers in selective solvents, the characteristic sizes of a polymeric micelle, i.e., the radius of the core and the thickness of the corona, are expressed as scaling laws with respect to the degrees of polymerization of each block.[1,42−45] For a copolymer AB in a solvent selective (good) for B, different regimes for the scaling have been identified, depending on the ratios between N_A and N_B or equivalently between R_C and R_H. N_A and N_B denote the degrees of polymerization of blocks A and B. The two opposite regimes are the crew-cut and the starlike micellar regimes, which are obtained respectively when $N_A \gg N_B$ and $N_A \ll N_B$. For crew-cut micelles, the overall size of the aggregate is dominated by that of the core, so $R_C \sim R_{II}$, and for starlike particles it is the reverse, $R_C/R_H < 0.1$.[44,45] As revealed by the data of Table 3, the core−shell structures of the colloidal complexes studied in this work are neither crew-cut nor stars. They rather belong to an intermediate regime which is characterized by values of R_C/R_H around 0.2−0.5.[45] We recall below the scaling laws for the aggregation number N_{Agg} and for the corona thickness $h = R_H - R_C$, as derived in the intermediate regime:[42]

$$N_{Agg} \sim N_A^{2} N_B^{-18/11}, \quad h \sim N_{Agg}^{1/9} N_A^{-2/9} N_B \qquad (3)$$

From geometrical arguments and in the strong segregation limit approximation, the radius of the core is found to scale as $R_C \sim (N_{Agg}N_A)^{1/3}$. At fixed N_B in eq 3, the aggregation number and the core radius increase with increasing N_A (with exponents 2 and 1, respectively). Similarly, at fixed N_A and increasing N_B, the core radius of the polymeric micelles decreases as $R_C \sim N_B^{-6/11}$, whereas the brush thickness increases as $\sim N_B^{9/11}$. It should be noted that as far the first relationship in eq 3 is concerned, exponents slightly higher than −18/11 have been found experimentally ($N_{Agg} \sim N_B^{-0.5}$ in refs 43 and 45, and $N_{Agg} \sim N_B^{-0.8}$ in ref 44). In all examples known, however, the exponent of the $N_{Agg}(N_B)$ scaling is negative. With the help of the data in Table 3, we are able to check qualitatively whether the colloidal complexes made from charged copolymers and surfactants exhibit similar variations.

(i) From the data in Table 3, we observe that the radius of the core depends essentially on the degree of polymerization of the polyelectrolyte block. For PANa(14)-*b*-PAM(70) and PANa(14)-*b*-PAM(140) we have found $R_C \sim 70$ Å, and for PANa(69)-*b*-PAM(420) and PANa(69)-*b*-PAM(840) $R_C = 130-140$ Å. This is in agreement with the above predictions (although the growth in R_C is slower than the predicted $R_C \sim N_A^{1}$).

(ii) With a neutral chain increasing by a factor 2 in the above examples, the core radius should be diminished by 30% ($\sim 1-2^{-6/11}$). This variation is not observed experimentally. On the contrary, the molecular weight of the neutral chain does not seem to be a relevant parameter for the core.

(iii) The overall size of the aggregates as deduced from R_H increases with increasing molecular weights of the copolymer. Figure 13, which shows R_H vs M_w for the six polymers considered, illustrates this tendency. This result is in qualitative agreement with eq 3, assuming that the variation of the corona thickness as a function of N_B will be the dominant contribution. These comparisons suggest finally that colloidal complexes made from oppositely charged copolymers and surfactants do not follow the same scaling properties as polymeric micelles. More experiments using e.g. monodisperse polymers should provide evidences for specific dependences.

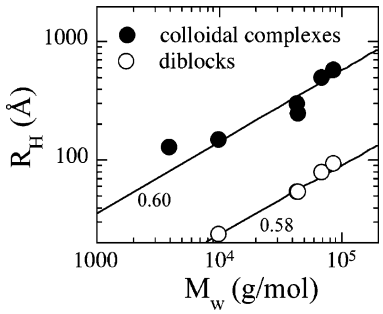

Figure 13. Hydrodynamic radius R_H of colloidal complexes made from the six diblocks copolymers studied and plotted as a function of the molecular weight of single chains. The data for the single chains as well as power law dependences with exponents 0.6 and 0.58 are also represented.

V. Conclusion

The structure of the colloidal complexes resulting from electrostatic association has been investigated by means of light, neutron, and X-ray scattering. With the present study, we have supplemented the description of the complexation between oppositely charged surfactant and copolymers with new features. Polyelectrolyte−neutral diblock copolymers associate with oppositely charged surfactants to form core−shell colloids in the range 25−100 nm. This has been found here for weak and strong polyelectrolyte blocks and for blocks which can be either positively or negatively charged (see Figures 6 and 9). The copolymers investigated are asymmetric and characterized by a rather large neutral block. For all copolymer/surfactant systems, there exists a critical mixing ratio Z_C above which the complexation, i.e., the formation of a hierarchical structure, takes place. Z_C is comprised between 0.1 and 1 for the copolymers investigated here, in agreement with previous studies.[16] Block copolymers with different molecular weights have been investigated and compared. From a quantitative analysis of the scattering intensities, we have found that the radius of the core depends essentially on the degree of polymerization of the polyelectrolyte block and not (or only weakly) on that of the neutral chain. The scaling laws observed for amphiphilic diblocks in selective solvents with similar asymmetries between the hydrophobic and hydrophilic blocks do not seem to apply to the present systems. Finally, a comparison of the structure peaks obtained by small-angle neutron and X-ray scattering enables us to conclude unambiguously about the structure of the core. The surfactant micelles within the cores are disordered; i.e., they do not exhibit any crystalline or translational order. This is an important result since it shows that once bound to a neutral chain, a polyelectrolyte chain will not necessarily complex surfactants according to a unique structure, as for instance the *Pm*3*n* cubic structure found in PANa(420)/DTAB precipitates. This is also true for the system PTEA(41)-*b*-PAM(420) with SDS. With the homopolyelectrolyte PTEA(41), the dense precipitate displays an hexagonal arrangement of infinitely long SDS cylinders, whereas with the diblock, the SDS self-assemble in spherical micelles. In a forthcoming paper, we will show how to derive the compositions

in terms of numbers of micelles and diblocks per colloid from scattering data.

Acknowledgment. We thank C. Gérardin, W. Loh, M. Morvan, L. Novaki, J. Oberdisse, R. Schweins, A. Sehgal, and K. Wong for many useful discussions. Mathias Destarac from the Centre de Recherches d'Aubervilliers (Rhodia, France) is acknowledged for providing us the polymers. We thank the Laboratoire Léon Brillouin (Saclay, France) and the Institute Laue-Langevin, (Grenoble, France) for their technical and financial support. We are also grateful to one of the referees for the comments on the line broadening due to the limited crystallite sizes. This research was carried out in part at the National Synchrotron Light Source, Brookhaven National Laboratory, which is supported by the U.S. Department of Energy, Division of Materials Sciences and Division of Chemical Sciences, under Contract DE-AC02-98CH10886. It is supported by Rhodia and by the Centre de la Recherche Scientifique in France.

References and Notes

(1) Riess, G. *Prog. Polym. Sci.* **2003**, *28*, 1107−1170.
(2) Cölfen, H. *Macromol. Rapid Commun.* **2001**, *22*, 219−252.
(3) Kataoka, K.; Togawa, H.; Harada, A.; Yasugi, K.; Matsumoto, T.; Katayose, S. *Macromolecules* **1996**, *29*, 8556−8557.
(4) Harada, A.; Kataoka, K. *Science* **1999**, *283*, 65−67.
(5) Harada, A.; Kataoka, K. *Macromolecules* **1998**, *31*, 288−294.
(6) Harada, A.; Kataoka, K. *Langmuir* **1999**, *15*, 4208−4212.
(7) Bronich, T. K.; Kabanov, A. V.; Kabanov, V. A.; Yui, K.; Eisenberg, A. *Macromolecules* **1997**, *30*, 3519−3525.
(8) Bronich, T. K.; Cherry, T.; Vinogradov, S.; Eisenberg, A.; Kabanov, V. A.; Kabanov, A. V. *Langmuir* **1998**, *14*, 6101−6106.
(9) Bronich, T. K.; Popov, A. M.; Eisenberg, A.; Kabanov, V. A.; Kabanov, A. V. *Langmuir* **2000**, *16*, 481−489.
(10) Li, Y.; Gong, Y.-K.; Nakashima, K.; Murata, Y. *Langmuir* **2002**, *18*, 6727−6729.
(11) Bouyer, F.; Gérardin, C.; Fajula, F.; Puteaux, J.-L.; Chopin, T. *Colloids Surf. A* **2003**, *217*, 179−184.
(12) Gérardin, C.; Sanson, N.; Bouyer, F.; Fajula, F.; Puteaux, J.-L.; Joanicot, M.; Chopin, T. *Angew. Chem., Int. Ed.* **2003**, *42*, 3681−3685.
(13) Jeong, J. H.; Kim, S. W.; Park, T. G. *Bioconjugate Chem.* **2003**, *14*, 473−479.
(14) Bronstein, L. M.; Platonova, O. A.; Yakunin, A. N.; Yanovskaya, I. M.; Dembo, A. T.; Makhaeva, E. E.; Mironov, A. V.; Khokhlov, A. R. *Langmuir* **1998**, *14*, 252−259.
(15) Hervé, P.; Destarac, M.; Berret, J.-F.; Lal, J.; Oberdisse, J.; Grillo, I. *Europhys. Lett.* **2002**, *58*, 912−918.
(16) Berret, J.-F.; Cristobal, G.; Hervé, P.; Oberdisse, J.; Grillo, I. *Eur. J. Phys. E* **2002**, *9*, 301−311.
(17) Skepo, M.; Linse, P. *Macromolecules* **2003**, *36*, 508−519.
(18) Castelnovo, M. *Europhys. Lett.* **2003**, *62*, 841−847.
(19) Allen, R. J.; Warren, P. B. *Europhys. Lett.* **2003**, *64*, 468−474.
(20) Berret, J.-F.; Hervé, P.; Aguerre-Chariol, O.; Oberdisse, J. *J. Phys. Chem. B* **2003**, *107*, 8111−8118.
(21) Cleasson, P. M.; Bergström, M.; Dedinaite, A.; Kjellin, M.; Legrand, J.-F.; Grillo, I. *J. Phys. Chem. B* **2000**, *104*, 11689−11694.
(22) Taton, D.; Wilczewska, A.-Z.; Destarac, M. *Macromol. Rapid Commun.* **2001**, *22*, 1497−1503.
(23) Destarac, M.; Bzducha, W.; Taton, D.; Gauthier-Gillaizeau, I.; Zard, S. Z. *Macromol. Rapid Commun.* **2002**, *23*, 1049−1054.
(24) Doi, M.; Edwards, S. F. *The Theory of Polymer Dynamics*; Clarendon Press: Oxford, 1986.
(25) Brandrup, J., Immergut, E. H., Grulke, E. A., Eds.; *Polymer Handbook*, 4th ed.; John Wiley and Sons: New York, 1999.
(26) Cotton, J.-P., Nallet, F., Eds.; *Diffusion des Neutrons aux Petits Angles*; EDP Sciences: Les Ulis, France, 1999; Vol. 9.
(27) Sokolov, E.; Yeh, F.; Khokhlov, A.; Grinberg, V. Y.; Chu, B. *J. Phys. Chem. B* **1998**, *102*, 7091−7098.
(28) Zhou, S.; Yeh, F.; Burger, C.; Chu, B. *J. Phys. Chem. B* **1999**, *103*, 2107−2112.
(29) Ashbaugh, H. S.; Lindman, B. M. *Macromolecules* **2001**, *34*, 1522−1525.
(30) Kogej, K.; Evmenenko, G.; Theunissen, E.; Berghmans, H.; Reynaers, H. *Langmuir* **2001**, *17*, 3175−3184.
(31) Svensson, A.; Topgaard, D.; Piculell, L.; Söderman, O. *J. Phys. Chem. B* **2003**, *107*, 13241−13250.
(32) Bergström, M.; Kjellin, U. R. M.; Cleasson, P. M.; Pedersen, J. S.; Nielsen, M. M. *J. Phys. Chem. B* **2002**, *106*, 11412−11419.
(33) Ilekti, P.; Piculell, L.; Tournilhac, F.; Cabane, B. *J. Phys. Chem. B* **1998**, *102*, 344−351.
(34) Ilekti, P.; Martin, T.; Cabanne, B.; Piculell, L. *J. Phys. Chem. B* **1999**, *103*, 9831−9840.
(35) Pedersen, J. S.; Gerstenberg, M. C. *Macromolecules* **1996**, *29*, 1363−1365.
(36) Pedersen, J. S.; Svaneborg, C. *Curr. Opin. Colloid Interface Sci.* **2002**, *7*, 158−166.
(37) Hansson, P. *Langmuir* **2001**, *17*, 4167−4179.
(38) Bertin, A.; Hervé, P. Personal communication, 2000.
(39) Pedersen, J. S.; Gerstenberg, M. C. *Macromolecules* **1996**, *29*, 1363−1365.
(40) Warren, B. E. *X-Ray Diffraction*; Dover Publications: New York, 1969.
(41) Burgh, S. v. d.; Keizer, A. d.; Stuart, M. A. C. Submitted for publication in 2003.
(42) Halperin, A.; Alexander, S. *Macromolecules* **1989**, *22*, 2403−2412.
(43) Nagarajan, R.; Ganesh, K. *J. Chem. Phys.* **1989**, *90*, 5843−5856.
(44) Förster, S.; Zisenis, M.; Wenz, E.; Antonietti, M. *J. Chem. Phys.* **1996**, *104*, 9956−9970.
(45) Willner, L.; Pope, A.; Allgaier, J.; Monkenbusch, M.; Lindner, P.; Richter, D. *Europhys. Lett.* **2000**, *51*, 628−634.

MA0498722